Magnetic spectrum of the two-dimensional antiferromagnet La_2CoO_4 studied by inelastic neutron scattering

P. Babkevich,[1, 2, *] D. Prabhakaran,[1] C. D. Frost,[3] and A. T. Boothroyd[1]

[1] Department of Physics, Oxford University, Oxford, OX1 3PU, United Kingdom
[2] Laboratory for Neutron Scattering, Paul Scherrer Institut, CH-5232 Villigen PSI, Switzerland
[3] ISIS Facility, Rutherford Appleton Laboratory, Didcot, Oxon., OX11 0QX, United Kingdom
(Dated: November 29, 2010)

We report measurements of the magnetic excitation spectrum of the layered antiferromagnet La_2CoO_4 by time-of-flight neutron inelastic scattering. In the energy range probed in our experiments (0–250 meV) the magnetic spectrum consists of spin-wave modes with strong in-plane dispersion extending up to 60 meV, and a nearly dispersionless peak at 190 meV. The spin-wave modes exhibit a small (~ 1 meV) dispersion along the magnetic zone boundary. We show that the magnetic spectrum can be described very well by a model of a Heisenberg antiferromagnet that includes the full spin and orbital degrees of freedom of Co^{2+} in an axially-distorted crystal field. The collective magnetic dynamics are found to be controlled by dominant nearest-neighbour exchange interactions, strong XY-like single-ion anisotropy and a substantial unquenched orbital angular momentum.

I. INTRODUCTION

The evolution from antiferromagnetism to high-temperature superconductivity with carrier doping of the layered copper oxides[1] has inspired a vast literature on the electronic, structural, dynamical, and chemical properties of related materials. It has become clear from these studies that superconductivity and commensurate antiferromagnetic order are only two out of many different competing ordering tendencies found in systems of strongly interacting electrons.

Among other forms of order found in doped Mott insulators are nematic phases characterised by unidirectional density-wave states involving combined charge and spin order. Such 'striped' phases were first identified many years ago in hole-doped $(La,Nd)_2CuO_4$ (Ref. 2) and La_2NiO_4 (Refs. 3–6), but their significance for high-temperature superconductivity has been the subject of a continuing debate. Although much of the focus has been on the cuprates, the nickelates have contributed to this debate on account of their relatively well correlated and stable stripe order which is amenable to experimental investigation. One drawback, however, is that holes localised on Ni^{3+} ions in hole-doped La_2NiO_4 carry a spin which can interact magnetically both with other spins in the charge stripes and with the surrounding antiferromagnetic matrix of Ni^{2+}. The influence of these interacting magnetic degrees of freedom on the properties of stripes in nickelates has yet to be fully evaluated, but spin correlations associated with both Ni sites have been observed[7] and there remain some unexplained features in the spin excitation spectra.[8]

Recently, evidence has been presented for the existence of stripe phases in the layered cobaltate system $La_{2-x}Sr_xCoO_4$ (Ref. 9), which is isostructural with hole-doped La_2CuO_4 and La_2NiO_4. Neutron diffraction measurements on half-doped ($x = 0.5$) La_2CoO_4 show clear evidence for a charge ordering of Co^{2+} and Co^{3+} ions in a checkerboard pattern below $T_{co} \approx 825$ K, with an an-tiferromagnetic ordering transition at a much lower temperature $T_N \sim 60$ K.[10–12] The antiferromagnetic order in $La_{2-x}Sr_xCoO_4$ in the range $0.3 < x < 0.6$ was observed to be periodically modulated with the modulation wavevector nearly proportional to x,[9] a characteristic of the stripe phase found in $La_{2-x}Sr_xNiO_4$. The Sr-doped cobaltate system has an advantage over the nickelates in that for the compositions in which stripe-like magnetic correlations occur there is evidence to suggest that the Co^{3+} ions adopt the low spin ($S = 0$) state at low temperatures and are therefore not magnetically active.[13–15] Hence, the layered cobaltates offer the chance to investigate the fundamental interactions and excited states of an ordered stripe phase in which the doped holes do not possess low-energy spin degrees of freedom.

Attempts to understand the electronic phases in $La_{2-x}Sr_xCoO_4$ will require some basic knowledge of the parent antiferromagnet La_2CoO_4. Although the crystal structure and magnetic order of La_2CoO_4 have been studied in detail,[16] no measurements of the magnetic excitation spectrum have been published before now.

In this paper we present high-resolution measurements of the magnetic spectrum of $La_2CoO_{4+\delta}$ ($\delta \approx 0$) by neutron inelastic scattering. The methodology relates closely to that employed in a recent investigation carried out on the half-doped cobaltate $La_{1.5}Sr_{0.5}CoO_4$ (Ref. 15). The data presented here on La_2CoO_4 extend up to 250 meV in energy and reveal spin-wave-like excitations with a bandwidth of 60 meV. At much higher energies, there are excitations of a localised character. A good description of the data is achieved with a spin-wave model for a quasi-two-dimensional antiferromagnet that includes the full spin and orbital degrees of freedom of the Co^{2+} ions. The results show that La_2CoO_4 has dominant nearest-neighbour exchange interactions, although a weak dispersion along the zone boundary indicates that more distant interactions or non-linear terms in the Hamiltonian are not negligible. The anisotropy is strongly XY-like but there is also a weak in-plane anisotropy.
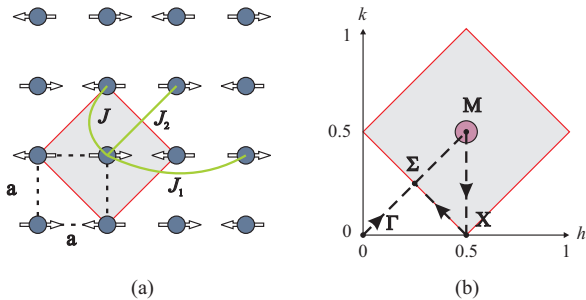
FIG. 1. (a) In-plane magnetic structure of La_2CoO_4. The dashed square shows the conventional $I4/mmm$ unit cell of the HTT phase, and the filled square represents the magnetic unit cell, which coincides with the $\sqrt{2} \times \sqrt{2}$ chemical unit cell of the LTT phase. The exchange interactions used to model the magnetic spectrum are indicated. (b) Diagram of the reciprocal space lattice corresponding to the $I4/mmm$ cell. The filled square indicates the magnetic Brillouin zone centered on $(0.5, 0.5)$. The dashed lines show the path through reciprocal space along high-symmetry directions used for detailed analysis of the magnetic excitation spectrum — see Fig. 5.

II. CRYSTAL AND MAGNETIC STRUCTURE

In common with the stoichiometric La_2CuO_4 and La_2NiO_4 compounds, La_2CoO_4 exhibits three different structural phases:[16] (i) $T > T_1$ high-temperature tetragonal (HTT), space group $I4/mmm$; (ii) $T_2 < T < T_1$ low-temperature orthorhombic (LTO), space group $Cmca$; (iii) $T < T_2$ low-temperature tetragonal (LTT), space group $P4_2/ncm$. The structural transition temperatures for La_2CoO_4 are $T_1 \approx 900\,K$ (Ref. 9) and $T_2 = 120 - 135\,K$ (Ref. 16). The latter is reported to be first order. Throughout this paper we shall use the conventional $I4/mmm$ unit cell as a basis for the reciprocal lattice. The low temperature lattice constants referred to this cell are $a = b = 3.91\,\text{Å}$ and $c = 12.6\,\text{Å}$. The true LTT unit cell has in-plane dimensions which are $\sqrt{2} \times \sqrt{2}$ larger than those of the $I4/mmm$ pseudo-cell — see Fig. 1(a).

The transition to magnetic order occurs at $T_N \approx 275\,K$, and a magnetic reorientation occurs at T_2 coincident with the LTO–LTT structural transition. The antiferromagnetic structure has an ordering wavevector $\mathbf{q}_m = (0.5, 0.5, 0)$, with ordered moments lying in the CoO_2 plane. Assuming collinear order, the difference between the magnetic structures in the LTT and LTO phases is that in the LTT phase the moments are perpendicular to $\mathbf{q}_m$ whereas in the LTO phase they are parallel to $\mathbf{q}_m$. The distinction between these structures depends on the relationship between adjacent layers. Another possibility is that the structure is collinear within the layers but the moment direction rotates by $\pm 90°$ from one layer to the next.[16] In the absence of inter-layer coupling all these structures have the same energy. As we did not observe any evidence in the excitation spectrum for inter-layer coupling we will treat the magnetic order as two-dimensional. Figure 1(a) shows the in-plane mag-

netic order with the moments arbitrarily chosen to point along the horizontal axis.

III. EXPERIMENTAL DETAILS

A single-crystal sample of La_2CoO_4 with a mass of approximately $5\,g$ was grown in Oxford by the optical floating-zone method. Polycrystalline La_2CoO_4 was prepared from high-purity ($>99.99\%$) La_2O_3 and Co_3O_4 by solid-state reaction. Stoichiometric amounts of the oxides were mixed and reacted at $1050°C$ for 48 hours under a flowing atmosphere of CO/CO_2 mixed in the ratio 1:10. A reducing atmosphere is needed to avoid the formation of $LaCoO_3$. The powder was re-ground and sintered at $1100°C$ in a flow of argon for a further 48 hours. No impurity phases could be detected in the product by x-ray powder diffraction. The La_2CoO_4 powder was isostatically pressed into rods of diameter $12\,mm$ and length $120\,mm$. The rods were sintered in an argon atmosphere at $1250°C$ for 24 hours. Crystal growth was carried out in a four-mirror image furnace (Crystal Systems Corporation) in flowing argon at a growth speed of approximately $2\,mm\,hr^{-1}$ with counter-rotation of the feed and seed rods at 25 rpm.

Crystals grown by this method contain an excess of oxygen. To achieve stoichiometry the as-grown crystal was annealed at $850°C$ for 72 hours in flowing CO/CO_2 (1:10 ratio). A fragment of the annealed crystal was ground to a powder and subjected to a thermogravimetric analysis. From the measured weight loss we determined the oxygen nonstoichiometry to be $\delta = -0.03 \pm 0.02$. This suggests that the crystal is close to the ideal stoichiometry, if anything slightly oxygen-deficient.

Magnetisation measurements were performed with a superconducting quantum interference device (SQUID) magnetometer (Quantum Design) on a small crystal cut from the same rod as the neutron scattering crystal. Measurements were made by the dc method with a measuring field of strength $1000\,Oe$ ($\mu_0 H = 0.1\,T$) applied along the crystallographic c axis. Zero-field-cooled (ZFC) data were recorded on warming after the sample had been initially cooled from $350\,K$ in zero applied field, and field-cooled (FC) data were recorded while cooling the sample from $350\,K$ in the measuring field.

Unpolarised-neutron inelastic scattering measurements were performed on the direct-geometry chopper spectrometer MAPS at the ISIS facility.[17] Neutron time-of-flight instruments with large position sensitive detector arrays such as MAPS allow sampling of vast regions of $(\mathbf{Q}, \omega)$ space simultaneously, where $\mathbf{Q}$ and $\hbar\omega$ are, respectively, the wavevector and energy transferred from the neutron to the sample. This is very advantageous in studies where the excitation spectrum is required throughout the Brillouin zone.

In preparation for the neutron measurements the La_2CoO_4 crystal was sealed in a thin-walled aluminium can containing helium exchange gas and aligned with the c axis parallel to the direction of the incident-neutron

beam. Cooling was provided by a closed-cycle refrigerator. Data were collected with incident-neutron energies of 51, 86, 111, 152 and 303 meV. The energy resolution was typically 5% of the incident energy (full width at half maximum) at zero energy transfer, decreasing slightly with increasing energy transfer. Under the chosen experimental conditions the wavevector resolution is largely determined by the divergence of the incident-neutron beam which is approximately 0.5°. Spectra from La_2CoO_4 were recorded at several temperatures between 6 and 300 K. Separate measurements of a standard vanadium sample were made at each incident energy to normalise the spectra and place them on an absolute intensity scale.

For presentation and analysis, the neutron data were transformed from raw time-of-flight spectra into an intensity map as a function of $\mathbf{Q}$ and $\hbar\omega$. With a fixed sample orientation, only three out of the four components of $(\mathbf{Q}, \omega)$ are independent. We chose the two in-plane wavevector components $(Q_x, Q_y) = (h, k) \times 2\pi/a$ and energy as the independent variables, which means that the out-of-plane wavevector $Q_z = l \times 2\pi/c$ varies implicitly with energy transfer. For a two-dimensional scattering system, however, there is no dispersion in the out-of-plane direction and the gradual variation of scattering intensity with Q_z can be included in a model (and was done so in this work). The justification for treating La_2CoO_4 as a two-dimensional magnetic system is that the magnetic spectra show no discernible periodic modulation in intensity with Q_z (i.e., with $\hbar\omega$).

In order to quantify the magnetic dispersion we performed a series of constant-energy and constant-wavevector cuts through the data volume along high-symmetry directions using the MSLICE software.[18] Before performing these cuts, data at symmetry-equivalent wavevectors were averaged to improve the signal.

IV. RESULTS

The temperature dependence of the FC and ZFC susceptibility ($\chi = M/H$) is shown in Fig. 2 (inset). Both curves show a change in slope at approximately 276 K consistent with the antiferromagnetic transition, and sharp anomalies at 124 K close to the temperature T_2 at which the LTO–LTT structural transition is expected. The onset of antiferromagnetism at $T_N \approx 276$ K is confirmed by the temperature dependence of the neutron diffraction intensity recorded at the magnetic Bragg peak position $(1.5, 1.5, 1)$, shown in Fig. 2. To estimate T_N we fitted the data to a power law $I \propto (1 - T/T_N)^{2\beta}$, assuming a Gaussian distribution of Néel temperatures about the mean value $\langle T_N \rangle$ with standard deviation of σ_T. This function was found to give a good description of diffraction data near T_N in Ref. 16. The parameters obtained from our data were $\langle T_N \rangle = 275.5(5)$ K, $\sigma_T = 1(1)$ K, and $\beta = 0.15(1)$. The transition temperatures measured on our sample are consistent with previously reported values of $T_N = 275$ K and $T_2 \approx 135$ K for a nominally stoichiometric crystal.[16] Although there is some discussion in
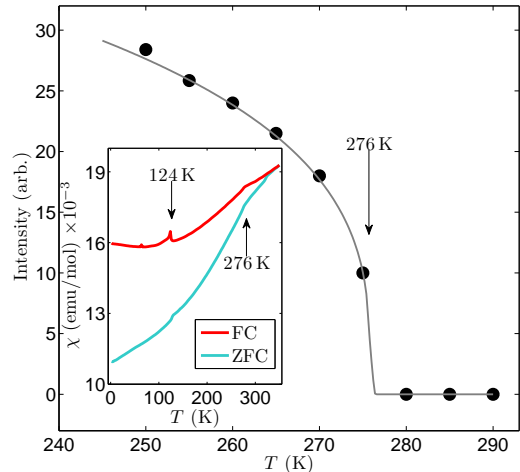

FIG. 2. Main figure: temperature dependence of the $(1.5, 1.5, 1)$ magnetic Bragg peak of La_2CoO_4 showing the onset of magnetic order at $T_N \approx 276$ K. The solid line shows a power law fit to data with a Gaussian distribution of Néel temperatures. Inset: field-cooled (FC) and zero-field-cooled (ZFC) magnetic susceptibility of La_2CoO_4 recorded with a measuring field of 1000 Oe applied parallel to the c axis. The magnetic ordering transition and the LTO–LTT structural transition are indicated by arrows.

the literature about the precise composition of La_2CoO_4 prepared under different conditions,[16,19–21] we can at the very least be confident that our crystal is close in composition to the one used in Ref. 16.

We note that the FC and ZFC susceptibility curves separate below 350 K, which is not expected in the paramagnetic phase. This indicates that the sample contains a small amount of ferromagnetic impurity. The FC–ZFC separation was not observed in the as-grown crystal. The most probable explanation is that a tiny amount of elemental Co was formed during the CO/CO_2 annealing step. This is consistent with the slight oxygen deficiency found from the thermogravimetric analysis. As there is no unexplained secondary signal in our neutron scattering spectra this impurity must be present in very small quantities so is of no consequence to our neutron results, but it does mean that the susceptibility curves shown in Fig. 2 contain a background signal in additional to the signal from pure La_2CoO_4.

We now turn to the neutron scattering spectra. Figure 3 provides an overview of the data collected at 6 K. Panels (a)–(c) are constant-energy slices at three different energies, and panels (g)–(i) are energy–$\mathbf{Q}$ slices to illustrate the magnetic dispersion. The spectrum is dominated by a spin-wave-like conical dispersion which rises from the in-plane antiferromagnetic ordering wavevector $\mathbf{q}_m = (0.5, 0.5)$ and equivalent positions [the M-points of the square-lattice Brillouin zone — see Fig. 1(b)]. This mode has a gap of approximately 10 meV at the M-point and rises to a maximum energy of 60 meV at the Σ-point on the Brillouin zone boundary. A much weaker branch, displaying an upwards dispersion with a minimum energy
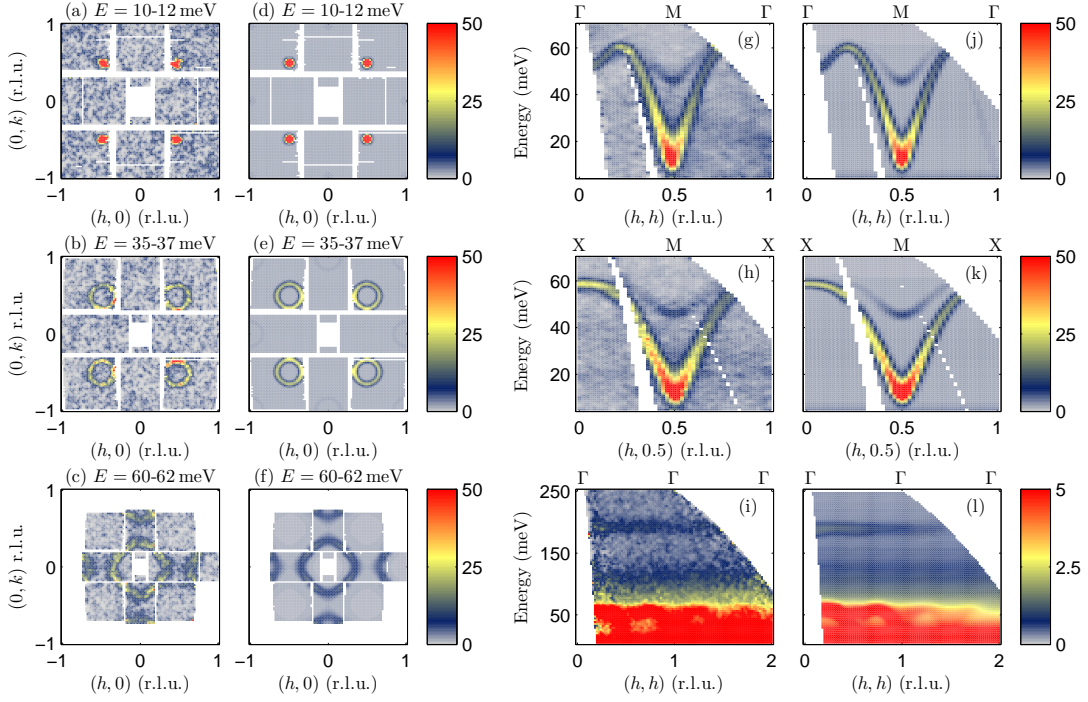
FIG. 3. Measured and simulated magnetic spectra of La_2CoO_4 at 6 K. Panels (a)–(c) show intensity maps averaged over 2 meV energy ranges centered on different energies as indicated, with the corresponding calculated spectra shown in (d)–(f). The magnetic dispersion along two high-symmetry directions is displayed in (g)–(i), with corresponding simulations in (j)–(l). Data in (a)–(h) were measured with an incident neutron energy $E_i = 86$ meV, while (i) was measured with $E_i = 303$ meV. The units of intensity indicated by the colourbars are $mb\,sr^{-1}\,meV^{-1}\,f.u.^{-1}$. The simulated spectra are calculated from the spin-orbital spin-wave model described in the text.
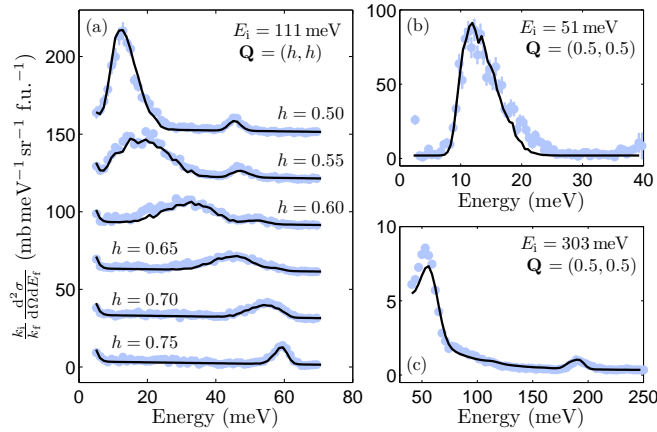

FIG. 4. Constant-$\mathbf{Q}$ cuts taken through the measured and simulated spectra. Panel (a) shows a series of cuts following the dispersion from the zone center $(0.5, 0.5)$ to the antiferromagnetic zone boundary at $(0.75, 0.75)$ measured with incident energy 111 meV. Panel (b) shows the spin gap of ~ 10 meV at $(0.5, 0.5)$ measured with an incident energy of 51 meV which gave an improved energy resolution. Panel (c) shows the measured and simulated excitation mode at ~ 190 meV. These data were obtained with $E_i = 303$ meV.

at M of 46 meV, corresponds to the first mode translated by $\mathbf{q}_m$. The large splitting of the modes at M shows that the anisotropy is strongly XY-like. The lower and upper

modes correspond to in-plane and out-of-plane fluctuations, respectively. Figure 3(i) shows data up to the maximum energy explored in our experiment. This reveals only one other significant feature — a band of scattering in a narrow range of energies close to 190 meV. We note that scattering from phonons is much weaker than magnetic scattering in the range of $\mathbf{Q}$ studied.

To give a different impression of the data we present in Fig. 4 examples of constant-$\mathbf{Q}$ cuts taken through the data volumes measured with incident energies $E_i = 51, 111$ and 303 meV. To extract the magnetic dispersion in a form suitable for fitting to a model we performed a large number of such constant-energy cuts at wavevectors along the reciprocal-space paths indicated in Fig. 1(b). The peaks in these plus some additional constant-wavevector cuts were fitted with Gaussian functions on a linear background. The peak centers determined this way are plotted along the high symmetry directions in Fig. 5.

An interesting behaviour is observed along the magnetic zone boundary: the energy of the magnon branch is not constant but varies by approximately 1.5 meV. As discussed below, this is significant because a dispersion along the zone boundary indicates a need to go beyond a linear spin-wave model with nearest-neighbour interactions only. To emphasise this effect, we show in Fig. 6(a) the energy and (b) the integrated intensity of the magnon peak along the entire length of a zone boundary (XΣX).
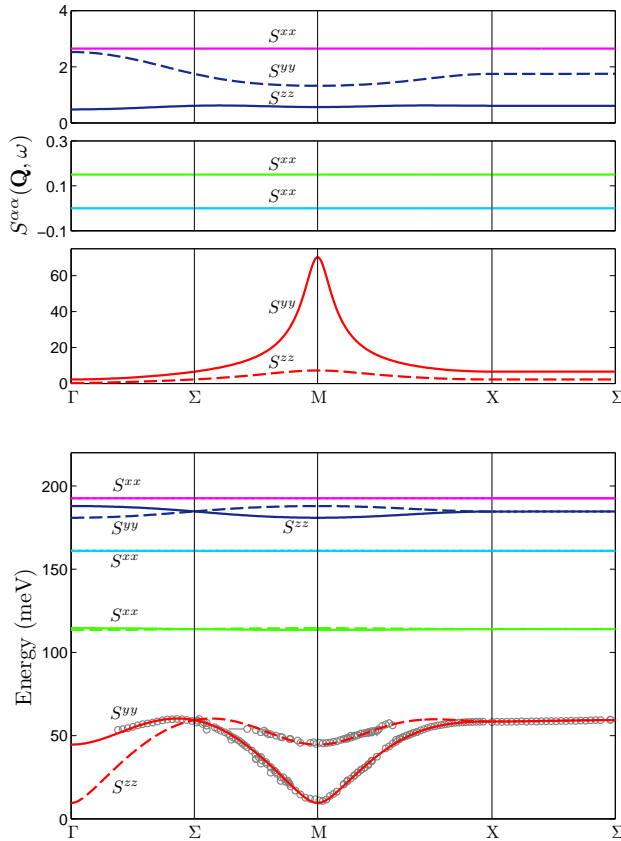
FIG. 5. The lower figure shows the dispersion of the magnetic excitations of La_2CoO_4 along high symmetry directions in the 2D Brillouin zone defined in Fig. 1. Open circles are points extracted from cuts through the measured data volume. The lines show the dispersion of the modes calculated with the many-level spin-wave model described in the text. The upper figure shows the response functions $S^{\alpha\alpha}$ for each mode calculated from the many-level model. The normalization of the response functions is per formula unit of La_2CoO_4.

V. ANALYSIS AND DISCUSSION

Magnetism in Co^{2+} compounds such as La_2CoO_4 is generally influenced to a significant degree by unquenched orbital angular momentum which is responsible for, among other things, the strong anisotropy in

the susceptibility observed in many such compounds. In a recent study[15] of the magnetic excitations in the half-doped cobaltate $La_{1.5}Sr_{0.5}CoO_4$, which is also an antiferromagnet, we developed a model to describe the magnetic spectrum including both the spin and orbital angular momentum of the Co^{2+} in the high-spin configuration ($3d^7$, $S = 3/2$, $L = 3$). The model is an advance over conventional (spin-only) spin-wave theory in that it includes level-mixing within the ^{2S+1}L term caused by the ligand and exchange fields, and hence the parameters that describe the single-ion anisotropy and exchange interactions are physically realistic. As far as the magnetic spectrum is concerned, the admixture of basis states means that excitations to levels above the first excited single-ion level can propagate and can be observed by neutron scattering. Moreover, the orbital component of the single-ion states needs to be included for an accurate calculation of the neutron cross section.

The model employs the Hamiltonian

$$\mathcal{H} = \sum_{\langle jk \rangle} J_{jk} \mathbf{S}_j \cdot \mathbf{S}_k$$

$$+ \sum_j \left[\sum_{l,m} B_l^m O_l^m(\mathbf{L}_j) + \lambda \mathbf{L}_j \cdot \mathbf{S}_j + \mathbf{H}_j^{\mathrm{a}} \cdot \mathbf{S}_j \right]. \quad (1)$$

The first term describes an isotropic Heisenberg exchange interaction between pairs of $S = 3/2$ spins. For La_2CoO_4 we include only the nearest-neighbour and next-nearest-neighbour exchange interactions J, J_1 and J_2, as defined in Fig. 1. The remaining terms in (1) are single-ion terms. The first of these represents the crystal (ligand) field acting on the Co^{2+} ions. The O_l^m are Stevens operator-equivalents with B_l^m the corresponding crystal-field parameters. The axially-distorted octahedral crystal field from the neighbouring O^{2-} ions is described by the operators O_2^0, O_4^0 and O_4^4. We kept the same values for the parameters B_4^0 and B_4^4 as found for $La_{1.5}Sr_{0.5}CoO_4$ in Ref. 15: $B_4^0 = -1.35\,\mathrm{meV}$ and $B_4^4 = -8.00\,\mathrm{meV}$. These are estimated from a point-charge calculation and scaled to match the cubic crystal field splitting observed in CoO.[22] The parameter B_2^0 controls the out-of-plane anisotropy and was adjusted to obtain a good fit to the magnetic spectrum. Its final value (see below) differs from that deduced for $La_{1.5}Sr_{0.5}CoO_4$ by only $\sim10\%$. The term $\lambda \mathbf{L} \cdot \mathbf{S}$ is the spin-orbit coupling. The coupling constant $\lambda = -18.7\,\mathrm{meV}$ used here has been deduced from reflectivity measurements of CoO by optical spectroscopy.[22] The final term $\mathbf{H}^{\mathrm{a}} \cdot \mathbf{S}$ represents a small uniaxial anisotropy which defines the in-plane orientation of the moments and produces a spin gap at the Γ-point (and, equivalently, the M-point). We chose the moments to lie along the x axis, and to achieve this the anisotropy field $\mathbf{H}^{\mathrm{a}}$ points along $+x$ on one of the antiferromagnetic sublattices and along $-x$ on the other.

The partial differential scattering cross-section depends on the response functions $S^{\alpha\alpha}(\mathbf{Q}, \omega)$ describing $\alpha\alpha$ magnetic correlations. In the dipole approximation the

The maximum in the dispersion at Σ is seen to coincide with a minimum in its intensity. Because the dispersion surface forms a ridge along the zone boundary care was taken to select an appropriately-sized box in $\mathbf{Q}$ over which to average the data so as to avoid systematic errors from the curvature of the dispersion surface while at the same time having good enough statistics to extract the peak energies and integrated intensities. Figure 6(c) shows energy cuts taken at an X-point and a Σ-point to illustrate the difference between the magnon peaks at the zone corner and zone edge.

relation is,[23]

$$\frac{k_i}{k_f}\frac{d^2\sigma}{d\Omega dE_f} = \left(\frac{\gamma r_0}{2}\right)^2 f^2(Q)\, e^{-2W} \sum_\alpha (1 - \hat{Q}_\alpha^2) S^{\alpha\alpha}(\mathbf{Q},\omega), \quad (2)$$

where

$$S^{\alpha\alpha}(\mathbf{Q},\omega) = \sum_j |\langle j|M^\alpha(\mathbf{Q})|0\rangle|^2 \delta[\omega - \omega_j(\mathbf{Q})]. \quad (3)$$

Here, k_i and k_f are initial and final neutron wavevectors, $(\gamma r_0/2)^2 = 72.8\,\text{mb}$, $f(Q)$ is the dipole magnetic form factor of Co^{2+}, e^{-2W} is the Debye-Waller factor which is close to unity at low temperatures, and $\hat{Q}_\alpha = Q_\alpha/|\mathbf{Q}|$ is the α component of a unit vector in the direction of $\mathbf{Q}$. The response function (per La_2CoO_4 f.u.) described in Eq. (3) takes into account both the spin and orbital magnetization $\mathbf{M} = -(\mathbf{L} + 2\mathbf{S})$ in the transition matrix element connecting the ground state to an excited mode j. The procedure to diagonalise the Hamiltonian (1) to obtain the dispersion and response functions of the magnetic modes is described in detail in Ref. 15.

The parameters of the model were refined from a fit to the measured dispersion carried out by a simulated-annealing algorithm. Because of the computer time required to diagonalise the Hamiltonian for the complete set of $2 \times \{(2L + 1)(2S + 1) - 1\} = 54$ excited states (twice the number of single-ion excited states because we have two magnetic sublattices) we restricted the number of observables included in the fit to just enough to represent all the important features of the data, including the high-energy signal at $\sim 190\,\text{meV}$. The parameters varied in the fit were B_2^0, J, J_1, J_2, and H^a. The best fit was achieved with parameters $B_2^0 = 14.6(1)\,\text{meV}$, $J = 9.69(2)\,\text{meV}$, $J_1 = 0.14(2)\,\text{meV}$, $J_2 = 0.43(1)\,\text{meV}$, and $H^a = 0.66(6)\,\text{meV}$. The calculated dispersion and response functions of the magnetic modes are shown in Fig. 5 together with the full set of data points for the lowest energy modes determined from the measurements. The agreement is seen to be very good. The fit indicates that the next-nearest-neighbour exchange constants J_1 and J_2 are very small but not zero. As a test, we repeated the fit with J_1 and J_2 fixed to zero and found that the quality of best fit worsened, as indicated by the standard goodness-of-fit parameter χ^2 per degree of freedom which increased from 4.5 to 11.1. Therefore, we believe that the obtained values of J_1 and J_2, though small, are significant.

To further visualise and assess the model we calculated intensity maps and cuts to simulate those obtained from the experiment. Figures 3 and 4 show the simulations alongside the corresponding experimental data. The quantity plotted is $(k_i/k_f)d^2\sigma/d\Omega dE_f$ per formula unit (f.u.), i.e., the partial differential cross section multiplied by a factor k_i/k_f as defined in Eq. (2). The dipole magnetic form factor of Co^{2+} and the $\mathbf{Q}$ orientation factor that determines the weighting of the different response functions are included in the simulated spectra. The simulations also take into account a number of other experimental factors: (i) we averaged over a 50:50 mixture of equivalent magnetic domains in which the ordered
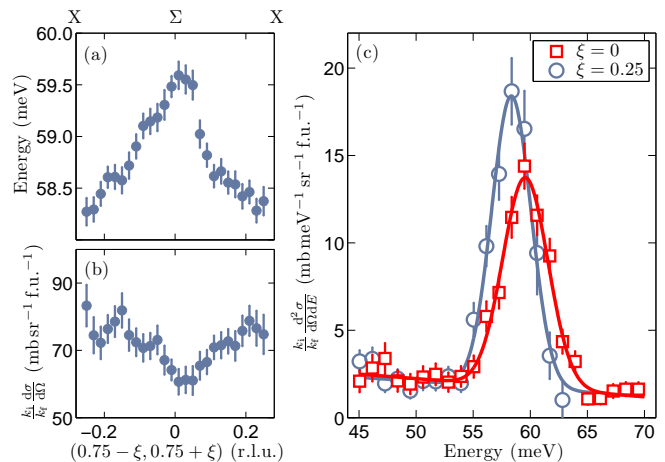

FIG. 6. Dispersion of the magnon peak along the magnetic zone boundary in La_2CoO_4. Variation of (a) the peak position and (b) the integrated intensity of the magnon peak in constant-$\mathbf{Q}$ cuts. (c) Constant-$\mathbf{Q}$ cuts at $\mathbf{Q} = (0.75, 0.75)$ and $(0.5, 1)$ fitted with Gaussian lineshapes. The data are from the run with incident energy 111 meV and sample temperature 6 K.

moments point along the x and y axes, respectively; (ii) the spectra are broadened in energy and wavevector by the estimated resolution of the MAPS spectrometer (see Sec. III); (iii) we included an estimate of the absorption and self-shielding of the neutron beam by the sample, which reduces the intensity by a factor of typically 0.65–0.80 depending on the incident neutron energy and $\hbar\omega$. An additional scale factor of 0.4 was applied uniformly to all calculated spectra in order to match the measured absolute scattering intensity.

The simulations show that the model provides a very good description of the entire observed spectrum of La_2CoO_4. The relative intensities of the magnetic excitations are reproduced to within 10–20 %, including the band of scattering at $\sim 190\,\text{meV}$, which from Fig. 5 is seen to originate from a mode with longitudinal (xx) character together with some less-intense transverse modes. Magnetic excitations are also present in the model at around ~ 115 and $\sim 165\,\text{meV}$ but are predicted to carry negligible spectral weight and are not observed — see Fig. 4(c). The additional scale factor of 0.4 needed to match the absolute intensity is similar to that required for $La_{1.5}Sr_{0.5}CoO_4$ (Ref. 15). It is accounted for partly by the size of the ordered moment. The observed ordered moment is $2.9\,\mu_B$ (Ref. 16) whereas the ordered moment in the (ionic) model is $4.1\,\mu_B$. The difference between observed and calculated moments may be an effect of covalency, which would also modify the magnetic form factor relative to the free ion form factor in such a way that could cause an additional reduction in intensity, as recently found in a cuprate chain compound.[24]

For reference, we also compared the low-energy part of the spectrum ($\hbar\omega < 60\,\text{meV}$) with standard linear spin-wave theory for an effective spin-$\frac{1}{2}$ antiferromagnet, which neglects the orbital component of the modes.

We used the same model as described in Ref. 15 in which the magnetic anisotropy is described by anisotropic nearest-neighbour exchange interactions $J_x = J(1 + \epsilon)$, $J_y = J$, and $J_z = J(1 - \delta)$. The parameters ϵ and δ control the in-plane and out-of-plane anisotropy, respectively. The more distant interactions J_1 and J_2 were included too, but because they are relatively small we treated these as isotropic. We found that the lower energy modes can be well described by this model. In fact, an equally good description of the data (as reflected in the value of χ^2) could be found with sets of parameters in which J_1 and J_2 are both positive or both negative: (i) $J = 9.89(1)\,\mathrm{meV}$, $J_1 = 0.04(1)\,\mathrm{meV}$, $J_2 = 0.13(1)\,\mathrm{meV}$, $\epsilon = 0.013(1)$, $\delta = 0.283(4)$, or (ii) $J = 8.30(6)\,\mathrm{meV}$, $J_1 = -0.35(2)\,\mathrm{meV}$, $J_2 = -0.63(3)\,\mathrm{meV}$, $\epsilon = 0.024(1)$, $\delta = 0.383(5)$. By contrast, the spin–orbital many-level model clearly favors the case with J_1 and J_2 both positive. The spin–orbital model can discriminate the two cases because of the inclusion of the higher excited levels. Only the parameter set with J_1 and J_2 both positive fits the low energy modes ($E < 60\,\mathrm{meV}$) *and* reproduces the peak in the spectrum at $\sim 190\,\mathrm{meV}$ and absence of any other measurable peaks between 60 and 250 meV. Another drawback of the effective spin-$\frac{1}{2}$ linear spin-wave model is that the intensities are not accurately described because of the neglect of the orbital degrees of freedom.

It is interesting to compare the magnetic spectrum of La_2CoO_4 with that of other two-dimensional, square-lattice, antiferromagnetic insulators, particularly in relation to the anomalous dispersion along the zone boundary. By "anomalous", we mean that the zone-boundary dispersion cannot be described within the framework of an antiferromagnetic spin-wave model in the linear approximation with only nearest-neighbour interactions. Inclusion of (i) interactions with more distant neighbours, or (ii) terms beyond the linear approximation, are two ways in which a zone-boundary dispersion can be obtained. Other layered antiferromagnets which exhibit zone-boundary dispersion include La_2CuO_4 (Refs. 25 and 26), $Sr_2Cu_3O_4Cl_2$ (Ref. 27) and $Cu(DCOO)_2 \cdot 4D_2O$ (CFTD, Refs. 28 and 29). These are all highly two-dimensional, $S = \frac{1}{2}$ Heisenberg antiferromagnets with almost isotropic interactions, and it is thought that the zone-boundary dispersion is caused by non-linear terms in the nearest-neighbour Heisenberg model. For example, in La_2CuO_4 a model with a four-spin ring exchange was employed,[25] and for CFTD a resonating-valence-bond model describing entangled spin-dimer states was proposed to explain the data.[29] Interestingly, the behaviour along the zone boundary is different in these two materials: in La_2CuO_4 both the energy and intensity are higher at X than at Σ, whereas in CFTD both the energy and intensity are higher at Σ than at X. In La_2CoO_4, on the other hand, the energy is a maximum at Σ while the intensity is a maximum at X (see Fig. 6). By contrast, there is virtually no zone-boundary dispersion at all in $S = 5/2$ square-lattice system Rb_2MnF_4, Ref. 30. In our analysis of La_2CoO_4 we found that although the zone boundary dispersion can be satisfactorily reproduced with an
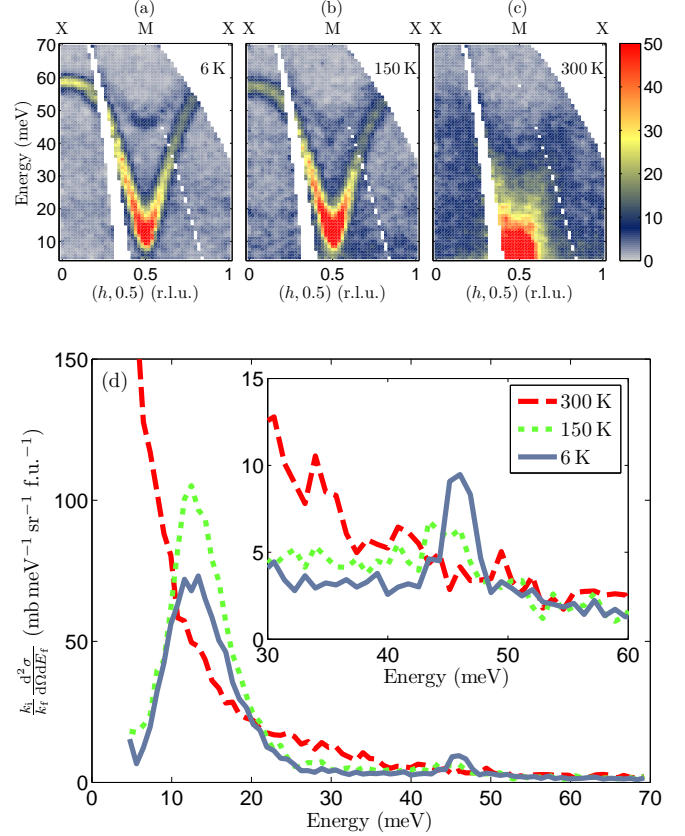

FIG. 7. Temperature dependence of the magnetic spectrum of La_2CoO_4. The upper panels (a)–(c) show intensity maps measured at 6, 150 and 300 K along the $(h, 0.5)$ direction. (d) Magnetic spectrum at the antiferromagnetic ordering wavevector $(0.5, 0.5)$ (M-point) measured at 6, 150 and 300 K. Inset: temperature evolution of the higher-energy magnon mode.

appropriate choice of J_1 and J_2, the corresponding intensity does not have the deep minimum at Σ found in the experiment [Fig. 6(b)]. Therefore, whether the zone boundary dispersion of La_2CoO_4 is due to interactions with more distant spins or arises from quantum effects in a non-linear nearest-neighbour model remains an open question.

Finally, we consider the temperature dependence of the magnetic spectrum. Figures 7(a)–(c) show maps of the magnetic scattering measured at $T = 6$, 150 and 300 K, and Fig. 7(d) displays constant-**Q** cuts at the magnetic zone center for the same temperatures. On increasing the temperature from 6 to 150 K the 11 meV peak increases in intensity due to the increasing thermal population but remains at the same energy, while the 46 meV peak broadens and shifts to lower energy [Fig. 7(d) inset]. Although La_2CoO_4 undergoes a first-order phase transition coincident with a magnetic reorientation at $T_2 \approx 125\,\mathrm{K}$, the in-plane lattice parameters in the LTO phase differ only slightly from those in the LTT phase, and the change in the magnetic structure only affects the stacking along the c axis. It is not surprising, therefore, that the transition does not significantly affect the magnetic spectrum. At

$T = 300$ K, the spectrum has become quasielastic and there are no longer any sharp inelastic peaks. This indicates the absence of long-range magnetic correlations for $T > T_N$.

VI. CONCLUSION

We have measured the excitation spectrum of single-crystal La_2CoO_4, an excellent realization of a two-dimensional Heisenberg antiferromagnet. We have combined the experimental results with numerical simulations to achieve a very good description of the magnetic spectrum throughout the entire Brillouin zone, up to an energy of 250 meV. The magnetic anisotropy is strongly XY-like, but a small uniaxial anisotropy is present which will make the low temperature magnetic properties Ising-like. An anomalous dispersion along the antiferromagnetic zone boundary is observed and can be reproduced by including exchange interactions beyond the nearest-neighbours but which could also be a manifestation of quantum fluctuations in a nearest-neighbour model.

ACKNOWLEDGMENTS

[*] peter.babkevich@physics.ox.ac.uk

[1] J. G. Bednorz and K. A. Müller, Z. Phys. B **64**, 189 (1986).

[2] J. M. Tranquada, B. J. Sternlieb, J. D. Axe, Y. Nakamura, and S. Uchida, Nature (London) **375**, 561 (1995).

[3] C. H. Chen, S. W. Cheong, and A. S. Cooper, Phys. Rev. Lett. **71**, 2461 (1993).

[4] J. M. Tranquada, D. J. Buttrey, V. Sachan, and J. E. Lorenzo, Phys. Rev. Lett. **73**, 1003 (1994).

[5] P. Wochner, J. M. Tranquada, D. J. Buttrey, and V. Sachan, Phys. Rev. B **57**, 1066 (1998).

[6] H. Yoshizawa, T. Kakeshita, R. Kajimoto, T. Tanabe, T. Katsufuji, and Y. Tokura, Phys. Rev. B **61**, R854 (2000).

[7] A. T. Boothroyd, P. G. Freeman, D. Prabhakaran, A. Hiess, M. Enderle, J. Kulda, and F. Altorfer, Phys. Rev. Lett. **91**, 257201 (2003).

[8] A. T. Boothroyd, D. Prabhakaran, P. G. Freeman, S. J. S. Lister, M. Enderle, A. Hiess, and J. Kulda, Phys. Rev. B **67**, 100407(R) (2003).

[9] M. Cwik, M. Benomar, T. Finger, Y. Sidis, D. Senff, M. Reuther, T. Lorenz, and M. Braden, Phys. Rev. Lett. **102**, 057201 (2009).

[10] I. A. Zaliznyak, J. P. Hill, J. M. Tranquada, R. Erwin, and Y. Moritomo, Phys. Rev. Lett. **85**, 4353 (2000).

[11] A. T. Savici, I. A. Zaliznyak, G. D. Gu, and R. Erwin, Phys. Rev. B **75**, 184443 (2007).

[12] K. Horigane, H. Hiraka, T. Uchida, K. Yamada, and J. Akimitsu, J. Phys. Soc. Jpn. **76**, 114715 (2007).

[13] N. Hollmann, M. W. Haverkort, M. Cwik, M. Benomar, M. Reuther, A. Tanaka, and T. Lorenz, New J. Phys. **10**, 023018 (2008).

[14] C. F. Chang, Z. Hu, H. Wu, T. Burnus, N. Hollmann, M. Benomar, T. Lorenz, A. Tanaka, H. J. Lin, H. H. Hsieh, C. T. Chen, and L. H. Tjeng, Phys. Rev. Lett. **102**, 116401 (2009).

[15] L. M. Helme, A. T. Boothroyd, R. Coldea, D. Prabhakaran, C. D. Frost, D. A. Keen, L. P. Regnault, P. G. Freeman, M. Enderle, and J. Kulda, Phys. Rev. B **80**, 134414 (2009).

[16] K. Yamada, M. Matsuda, Y. Endoh, B. Keimer, R. J. Birgeneau, S. Onodera, J. Mizusaki, T. Matsuura, and G. Shirane, Phys. Rev. B **39**, 2336 (1989).

[17] T. G. Perring and C. D. Frost, Neutron News **15**, 30 (2004).

[18] R. Coldea, MSLICE: a data analysis program for time-of-flight neutron spectrometers (2004).

[19] J. T. Lewandowski, R. A. Beyerlein, J. M. Longo, and R. A. McCauley, J. Am. Ceram. Soc. **69**, 699 (1986).

[20] R. A. Mohan Ram, P. Ganguly, C. N. R. Rao, and J. M. Honig, Mat. Res. Bull. **23**, 501 (1988).

[21] T. Kajitani, S. Hosoya, K. Hiraga, and T. Fukuda, J. Phys. Soc. Jpn. **59**, 562 (1990).

[22] C. Kant, T. Rudolf, F. Schrettle, F. Mayr, J. Deisenhofer, P. Lunkenheimer, M. V. Eremin, and A. Loidl, Phys. Rev. B **78**, 245103 (2008).

[23] G. L. Squires, *Introduction to the Theory of Thermal Neutron Scattering* (Dover Publications, Mineola, N.Y., 1996).

[24] A. C. Walters, T. G. Perring, J. S. Caux, A. T. Savici, G. D. Gu, C. C. Lee, W. Ku, and I. A. Zaliznyak, Nature Physics **5**, 867 (2009).

[25] R. Coldea, S. M. Hayden, G. Aeppli, T. G. Perring, C. D. Frost, T. E. Mason, S. W. Cheong, and Z. Fisk, Phys. Rev. Lett. **86**, 5377 (2001).

[26] N. S. Headings, S. M. Hayden, R. Coldea, and T. G. Perring, arXiv:1009.2915.

[27] Y. J. Kim, A. Aharony, R. J. Birgeneau, F. C. Chou, O. Entin-Wohlman, R. W. Erwin, M. Greven, A. B. Harris, M. A. Kastner, I. Y. Korenblit, Y. S. Lee, and G. Shirane, Phys. Rev. Lett. **83**, 852 (1999).

[28] H. M. Rønnow, D. F. McMorrow, R. Coldea, A. Harrison, I. D. Youngson, T. G. Perring, G. Aeppli, O. Syljuåsen, K. Lefmann, and C. Rischel, Phys. Rev. Lett. **87**, 037202 (2001).

[29] N. B. Christensen, H. M. Rønnow, D. F. McMorrow, A. Harrison, T. G. Perring, M. Enderle, R. Coldea, L. P. Regnault, and G. Aeppli, Proc. Natl. Acad. Sci. U.S.A. **104**, 15264 (2007).

[30] T. Huberman, R. Coldea, R. A. Cowley, D. A. Tennant, R. L. Leheny, R. J. Christianson, and C. D. Frost, Phys. Rev. B **72**, 014413 (2005).